



On-chip simultaneous rotation of large-scale cells by acoustically oscillating bubble array

Qiang Tang^{1,2} · Fei Liang¹ · Liang Huang¹ · Peng Zhao¹ · Wenhui Wang¹

Published online: 18 January 2020

© Springer Science+Business Media, LLC, part of Springer Nature 2020

Abstract

Bubbles locating in microfluidic chamber can produce acoustic streaming vortices by applying travelling surface acoustic wave oscillation in an ultrasonic range, which can be used to drive bio-samples to move within the flow field. In this paper, a strategy of bubble array configured in a large number of regularly arranged horseshoe structures is proposed to capture and rotate cells simultaneously. By modifying the geometric parameters of the horseshoe structure and microfluidic setting, high bubble homogeneity and cell trapping percentage was achieved. The simulation and experimental results of the bubble-induced streaming vortices were confirmed to be consistent. Through experiments, we achieved both in-plane and out-of-plane rotation of arrayed HeLa cells trapped by the bubbles. Out-of-plane rotation was used to reconstruct the 3D (three-dimensional) cell morphology, which was demonstrated to be useful in calculating cell geometry related parameters. We believe that this bubble array based cell rotation method is expected to be a promising tool for the investigation of bioengineering, biophysics, medicine, and cell biology.

Keywords Bubble array · Acoustofluidics · Cell rotation · Lab-on-a-chip

1 Introduction

Controlled manipulation of micro- and nano-scaled bio-samples like nematodes, cancer cells and exosomes in a microfluidic chamber is a current research hotspot in biotechnology (Ding et al. 2012; Gupta and Rezaei 2016; Perez-Gonzalez et al. 2016; Zhu et al. 2018; Johari et al. 2013; Ghanbari et al. 2012; Qiu et al. 2015) and has attracted great attention in the field of modern bioscience (Hu et al. 2013; Khoo et al. 2016; Kimura et al. 2018; Villone et al. 2018). Diverse methods for capturing, transporting, rotating, and separating numerous bio-samples with different shapes and sizes have been developed based on magnetic, dielectrophoretic,

optical, acoustophoretic, and hydrodynamic principles (Huang et al. 2018b; Lee et al. 2006; Ozkan et al. 2003; Torino et al. 2016; Urbansky et al. 2017; Jin et al. 2015; Mi et al. 2016; Cheng et al. 2016; Cheng et al. 2017; Tu et al. 2019; Zhang et al. 2019). Among these methods, acoustic streaming produced by ultrasonically oscillating bubbles is often considered to have the merits such as little physiological damage or invasion to manipulated bio-samples, low dependence on electromagnetic and optical properties of samples, simple and low-cost microfluidic platform, and so on (Marin et al. 2015; Wang et al. 2012). When travelling surface acoustic wave acts on a bubble in a microfluidic chamber, the gas-liquid interface can obviously enlarge vibration displacement and aggravate ultrasonic dissipation, leading to a nonlinear acoustic effect and inducing several vortices around the bubble, which is usually called bubble-induced acoustic streaming (Chen et al. 2017; Liu et al. 2002; Marmottant et al. 2006; Cui et al. 2019).

In the past decade, there have been numerous applications of bubble-induced acoustic streaming including fluid mixing, micro-object sorting and separation, propulsion of acoustic micro-motors, controlled precise rotational manipulation of bio-samples in lab-on-a-chip devices, to name just a few. One of the most commonly used functions of bubble-induced acoustic streaming is microfluidic mixing. Ahmed et al. (2009) and Xie et al. (2012) used a single acoustically-

Qiang Tang and Fei Liang are contributed equally.

Electronic supplementary material The online version of this article (<https://doi.org/10.1007/s10544-020-0470-1>) contains supplementary material, which is available to authorized users.

✉ Wenhui Wang
wwh@tsinghua.edu.cn

¹ State Key Laboratory of Precision Measurement Technology and Instrument, Department of Precision Instrument, Tsinghua University, Beijing 100084, China

² Faculty of Mechanical and Material Engineering, Huaiyin Institute of Technology, Huaian 223001, China

driven bubble anchored in a horseshoe structure to achieve fast mixing of two kinds of aqueous solutions in tens of milliseconds. Wang et al. (2013) achieved different mixing patterns by using a side-wall-trapped oscillating bubble modulated at different driving frequencies in a T-junction mixer. Ahmed et al. (2013) successfully realised the generation of spatial-temporal and tunable chemical gradient profiles using two or more acoustically driven oscillating bubbles positioned in a ladder-like arrangement by changing the applied voltage or frequency. Based on the effect that the smaller the size or density of a micro-object is, the larger its revolution radius in a vortex is, Wang et al. (2011), Zhou and Wang (2015), Thameem et al. (2016) sorted multiple micro-scaled particles of different sizes from different outlets by using a side-wall-trapped oscillating bubble. Patel et al. (2014), Garg et al. (2018) realised enrichment of larger targeted cells and separation of smaller unwanted cells simultaneously in a lateral cavity acoustic transducer device with a sequence of bubbles obliquely anchored in side walls. The propulsion force induced by asymmetric bubble-induced acoustic streaming distribution can be creatively applied in the design of acoustic micro-swimmers. Ahmed et al. (2015), Bertin et al. (2015) designed semi-enclosed bubble capsule and propelled bubble micro-swimmers in controlled 2-dimensional motions. Steady acoustic streaming vortices created by the oscillation of bubbles can stably rotate bio-samples. Ahmed et al. (2016) provided an acoustic, on-chip manipulation method that can realise in-plane or out-of-plane rotation of single polystyrene microparticles, HeLa cells and organisms like *C. elegans*. Läubli et al. (2017) also successfully demonstrated non-invasive trapping and controlled in-plane and out-of-plane rotational manipulation of *Lilium longiflorum* and *Arabidopsis thaliana* pollen grains using acoustically excited micro-bubbles.

Single cell analysis has attracted great attention recently due to the cell heterogeneity (Alberdi and Méresse 2017; Buettner et al. 2015; Tellez-Gabriel et al. 2016). It opens a new door for people to investigate into life sciences at single cell level through so called omics (genomics, transcriptomics, proteomics and metabolomics) assay (Mannello et al. 2012; Merrick et al. 2011; Wang and Bodovitz 2010). The upstream processing of single cell analysis includes cell sample preparation manipulations such as sorting, isolation, capture, transfer, rotation, and lysis (Benhal et al. 2014; Di Carlo et al. 2003; Gossett et al. 2012; Huang et al. 2017; Liu et al. 2011; Yu et al. 2014; He et al. 2019). During this course, it is also common to characterize the biophysical properties of single cells (Darling et al. 2007; Mohammadi et al. 2018; Rocha and Mesquita 2007; Feng et al. 2019; Tu et al. 2017; Wang et al. 2019; Pan et al. 2017). Cell rotation (Huang and Wang 2019; Huang et al. 2018a; Huang et al. 2016; Benhal et al. 2015; Benhal et al. 2014) is one such operation that works for pre-omics manipulation and analysis. To our knowledge, the

reported rotation works have yet made sufficient efforts to improve the throughput. That is, only one rotation unit has been configured in the existing devices for demonstration purpose.

In this paper, we describe an ultrasonically actuated, bubble-array-based method to rotate a large number of cells simultaneously and separately in controlled space. As a result, we can have ample rotating samples for observation and analysis at one time to increase the rotation throughput. Note in this work, all the bubble-generating structures were designed to be homogeneous as a proof of concept, but they can be different as well to make cells exhibit different rotation patterns. Steady acoustic streaming vortices are created by the oscillation of massive bubbles restrained by horseshoe structure array in a microfluidic chamber. The bubble-induced acoustic streaming is produced by a low-voltage travelling surface acoustic wave field. The whole operation only requires a single-layer polydimethylsiloxane (PDMS) chamber and a simple, low-cost, on-chip piezoelectric transducer near the PDMS chamber. In the process of device design, we modified the geometric parameters of horseshoe structure array, and microfluidic settings such as syringe pump speed and cell concentration to enhance bubble homogeneity and cell trapping. Few cells or cell populations near the gas-liquid interfaces can be captured to the vortex center and stably rotate in the bubble-induced acoustic streaming field. The rotation speed is proportional to the the square of the applied voltage of piezoelectric buzzer, and the rotation axis (i.e., in-plane or out-of-plane rotation) can be modulated by the input frequency. This bubble array platform enhances the space efficacy of the acoustofluidic chip, and facilitates simultaneous rotation of arrayed cells. Through a stack of two-dimensional contour image frames obtained from out-of-plane HeLa cell rotation, the 3D morphology was reconstructed to collect cellular geometric parameters like surface area, volume, ellipticity, and roughness. The bubble-array-based device actuated by ultrasonic excitation is expected to be a promising tool for the investigation of bio-sample phenotype characterization.

2 Experimental methods

2.1 Device design and fabrication

The device is designed to have the function of capturing and rotating massive cells simultaneously through bubble-induced acoustic streaming field. The generation and trapping of a large amount of micro-bubbles in a microfluidic chamber needs to be taken into consideration. On the basis of other groups' experience (Chindam et al. 2013; Xie et al. 2014; Yazdi and Ardekani 2012), we chose arrayed horseshoe structure (U-type dam structure made of PDMS) to guarantee the morphology consistency of trapped micro-bubbles. The

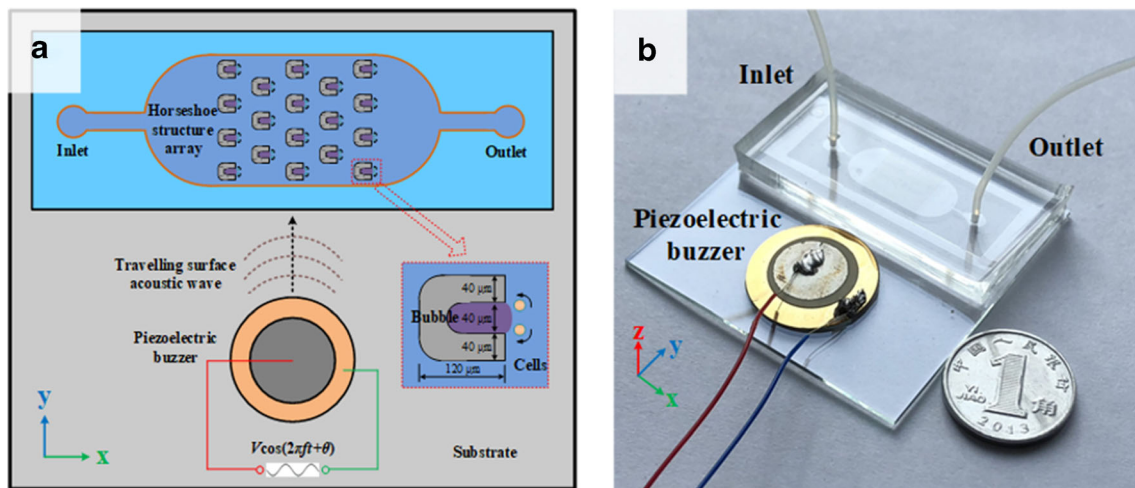


Fig. 1 Bubble array based acoustofluidic device for simultaneous rotation of massive cells using ultrasonic excitation. **(a)** Conceptual overview of the acoustofluidic chip, including its working principle of

rotational manipulation, structure, and typical geometric dimensions of each horseshoe structure unit. **(b)** Assembled real device

distribution and dimension parameter of horseshoe structure array was also modified to reduce the influence of solid-fluid boundaries on the micro-bubble generation and acoustic streaming field distribution.

The device consists of a PDMS-based single layer microfluidic chamber and a piezoelectric buzzer, as shown in Fig. 1. A single-layer PDMS microfluidic chamber (height: 60 μm , length: 19.6 mm, width: 9 mm) with pre-designated horseshoe structure array for micro-bubble trapping was fabricated using standard soft lithography and replica molding technique. A 60 μm -thick layer of negative photoresist (SU8-2060, MicroChem Corp., USA) was first spin-coated, photo patterned, and developed to obtain a chamber mold. Sylgard 184A Silicone Elastomer Base and Sylgard 184B Silicone Elastomer Curing Agent (Dow Corning, USA) were mixed at a 10:1 (weight:weight) ratio and poured on the mold. The uncured PDMS on the silicon mold was then degassed in a vacuum desiccator for 0.5 h to remove any air micro-bubbles and later cured at 80 $^{\circ}\text{C}$ for 2 h. After gently removing the cured PDMS from the mold, the inlets and the outlets were punched into the PDMS using a reusable biopsy punch. The microfluidic chamber device and a 50 \times 50 mm² micro-cover glass were treated with oxygen plasma for 60 s. Then, the PDMS device was bonded to the cover glass, and kept at 65 $^{\circ}\text{C}$ overnight. A piezoelectric buzzer (FT-12 T-18.5E, Yuansheng Electronics Co., Ltd., China) of 20 mm radius and 1 mm thickness was then attached to the glass slide adjacent to the chamber using modified Acrylate adhesive (Gelihaohao New Material Co., Ltd., China).

2.2 Device operation

The assembled device was mounted on an inverted optical microscope stage (CKX53, Olympus, Japan). PBS

(Phosphate Buffered Saline) together with samples (e.g., yeast cells, HeLa cells) was injected into the microfluidic chamber through a 2-mL syringe by an automated syringe pump (KD scientific, Legato 270, USA). Once the micro-bubbles were trapped in horseshoe structures via surface tension effect, the piezoelectric buzzer connecting to a function generator (AFG 3052C, Tektronix, USA) was activated to control the micro-bubble oscillation using a sine wave. The driving voltages used in the experiments were 1–10 V_{PP}. The working frequency for the rotational manipulation was adjusted by sweeping the frequency from 20 kHz to 200 kHz.

2.3 Image acquisition

The bubble-induced acoustic streaming vortex and bio-sample images were captured by Olympus imaging software using a CCD digital camera (DP80, Olympus, Japan), which was mounted on the C-port of the inverted microscope (CKX53, Olympus, Japan) and working at several selected special frequency points through frequency sweeping, e.g., 43 kHz for in-plane cell rotation and 56 kHz for out-of-plane cell rotation.

2.4 Cell culture and preparation

HeLa cells were cultured using Dulbecco's modified Eagles medium (DMEM) (Gibco, Grand Island, NY, USA) with 10% fetal bovine serum (FBS) (Gibco), 2% GlutaMax (Gibco) and 1% penicillin/streptomycin (Gibco) in a 5% CO₂ and 37 $^{\circ}\text{C}$ incubator (LabServ CO150, Fisher Scientific, USA). Cells were rinsed with PBS (Gibco) twice, and adherent cells were then lifted off by treating with trypsin for 5 min. The cell suspension was washed three times by centrifuging at 300 g for 5 min, removing the supernatant with a pipette, and re-suspending the cell pellet in PBS solution with different cell

concentrations. The cell suspension was finally injected into the microfluidic chamber with different propulsion speeds and time durations.

Instant dry yeast cells (Angel Yeast Co., Ltd., China) with an average diameter of 3 μm were directly suspended in de-ionized water with a final cell concentration of 1,000,000 cells/mL and were injected into the microfluidic chamber.

We chose yeast and HeLa cells in our experiment mainly due to their availability and suitability for demonstration. Both cells are typical, spherical, suspended cells. Yeast cells could be used as cheap tracer particles to visualize the streamline of bubble-induced acoustic streaming vortices. HeLa cells or cell clumps were easily accessible to verify the simultaneous rotation function of the device for typical mammalian cells in Fig. 2.

3 Experimental results and discussion

3.1 Bubble generation for two empirical array structures

The horseshoe shaped microstructures fabricated inside a microfluidic chamber can realise bubble trapping at different flow rates. However, the gas-liquid interfaces of trapped bubbles are influenced by the propulsion speed of syringe pump and propulsion duration according to our experiment. The extension length of bubble area outside the horseshoe structure decreases with the increase of propulsion speed and duration, and interface indentation may occur at a high flow rate and a long propulsion duration. According to literature (Ahmed et al. 2009, 2014; Chindam et al. 2013), a single air bubble can be trapped within the horseshoe structure due to the gas-liquid interface and the hydrophobic-hydrophilic interaction between the PDMS horseshoe structure and the fluid. The shape and size of the trapped bubble are mainly dependent on the horseshoe structure and the surface tension among

different gas-liquid-solid phases. Once the horseshoe structure is fixed, the surface tension plays the big role and would be affected by the horseshoe array arrangement but hardly formulated. Therefore, we proposed to make the bubble array homogeneous, and the initial choice of the corresponding horseshoe array design was to duplicate each horseshoe structure regularly in row and column as shown in Fig. 3.

The two kinds of horseshoe structure arrays were compared to improve the space efficacy of microfluidic chamber. The first design is a gridded array (Fig. 3a), where the x -directional and y -directional distances between two adjacent horseshoe structures are the same (120 μm). However, in the experiment, we found that bubbles along the direction of inflow field would often stick to the neighboring horseshoe structure, which greatly endangers the homogeneity and availability of bubbles. Thus, this kind of array design was abandoned. In order to avoid the interference between adjacent structures, we placed the horseshoe structure arrays in staggered ways with different x -directional spacing. However, for small horizontal spacing (180 μm in Fig. 3b while the y -directional spacing is the same), a large bubble sometimes forms somewhere inside the horseshoe structures. Based on the experiment, we finally chose the array design in Fig. 3c with a larger x -directional spacing of 360 μm while the y -directional spacing of 180 μm at the expense of space utilization, and found that about 90% horseshoe structures (totally 1643) in the microfluidic chamber can form workable bubbles for cell trapping and rotation. Through experiment, we found that a propulsion speed of 0.2 mm/s and a duration of 2 s for the syringe pump worked well to generate useful bubbles for the selected horseshoe structure.

3.2 Particle trajectory and streamline distribution

According to the simulation method of acoustic streaming field produced by bubble oscillation in the supplementary material (Ahmed et al. 2016; Bruus 2012; Lei 2017; Lei et al. 2018; Lighthill 1978; Tang et al. 2018; Xie et al. 2016), we

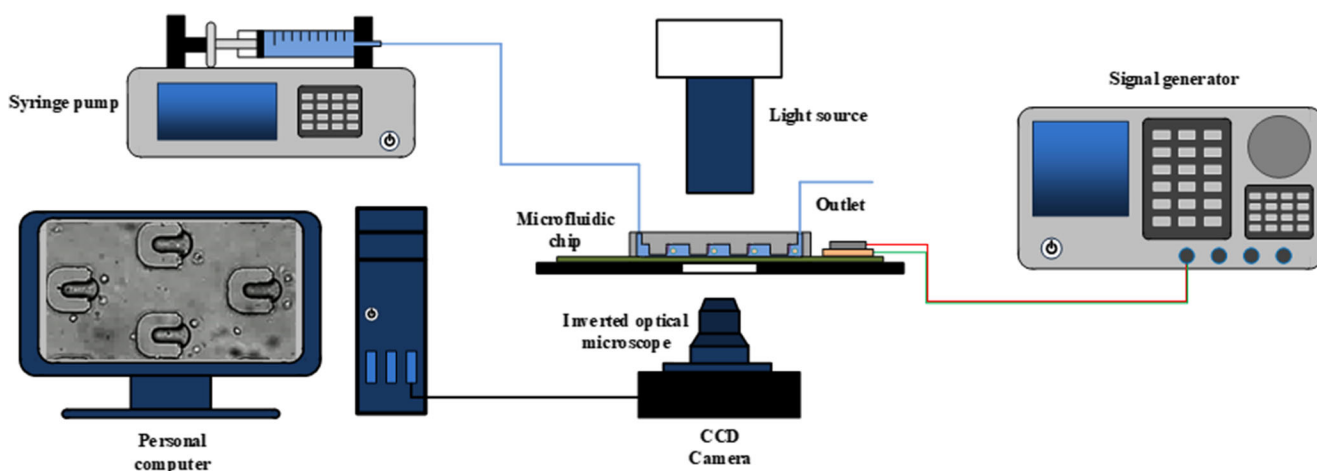


Fig. 2 Schematic of the experimental system

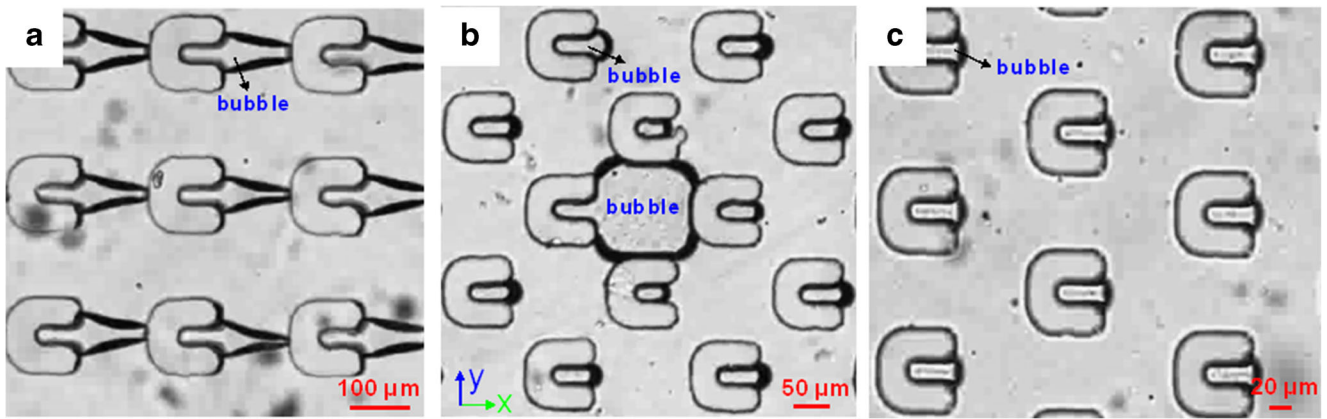


Fig. 3 Bubble generation for different horseshoe structure arrays. **(a)** Gridded array. Staggered array with a x-directional spacing of 180 μm **(b)** and 360 μm **(c)**

calculated the streaming patterns generated by a single bubble in the microfluidic chamber of dimensions $360 \times 360 \mu\text{m}^2$. The simulated acoustic streaming patterns are shown in

Fig. 4a, where the bubble is oscillating with the amplitude of 10 nm at 40 kHz. The color bar and arrows denote the magnitude and direction of acoustic streaming velocity,

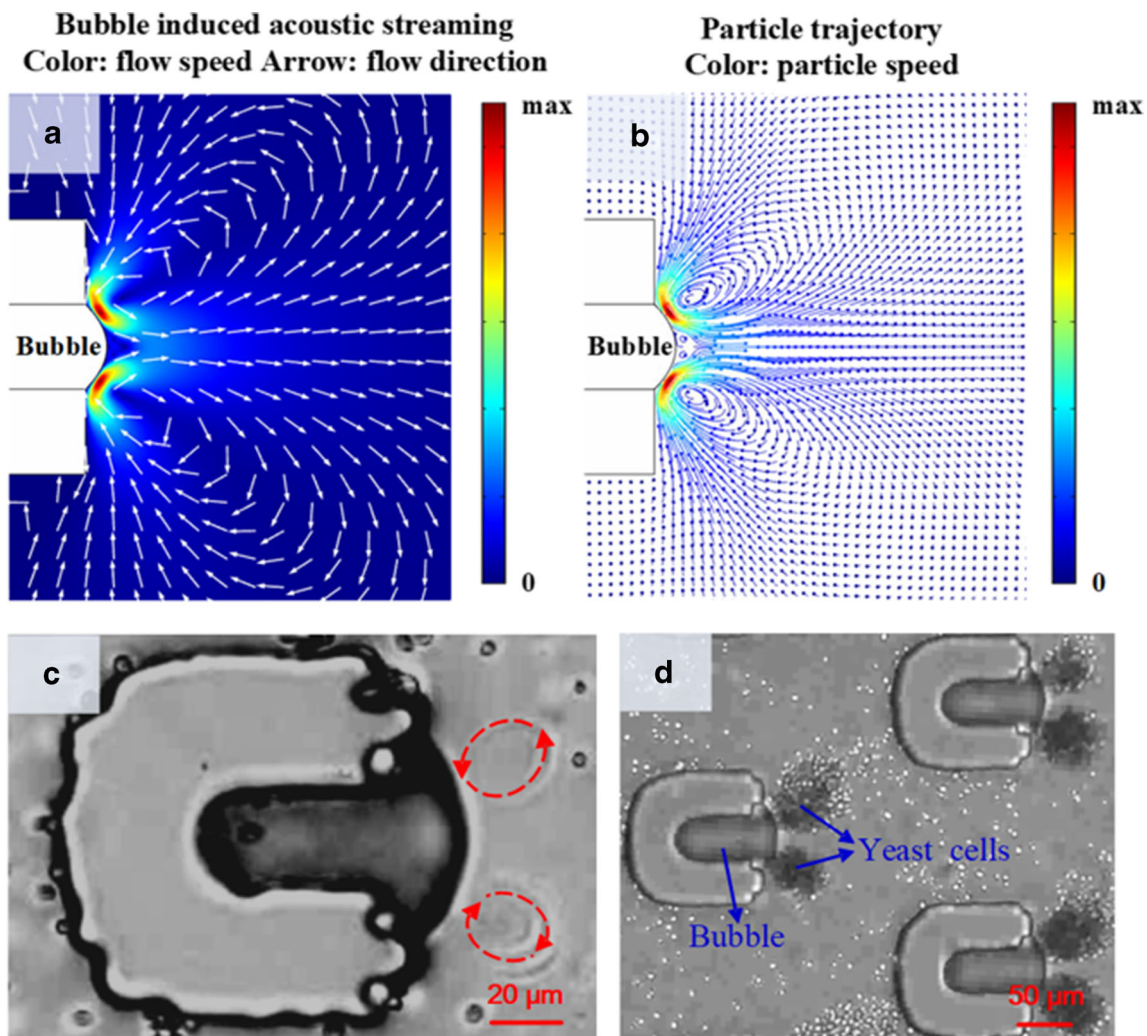


Fig. 4 Bubble-induced acoustic streaming field. **(a)** Simulated acoustic streaming pattern. **(b)** Simulated particle trajectory. **(c)** A bubble with a small amount of rotating yeast cells indicating the flow direction of

acoustic streaming vortices. **(d)** Bubbles with a large amount of yeast cells rotating in the acoustic streaming vortices

respectively. Two acoustic streaming vortices with opposite rotation orientations near the gas-liquid interface trapped by the horseshoe structure can be obviously noted from the FEM simulation result. The acoustic streaming field flows in from the gas-liquid-solid intersection and out from the central radiation surface of the gas-liquid interface. The areas with the largest acoustofluidic speed occur near the two gas-liquid-solid intersections of the horseshoe structure because of the obvious variation of sound field gradient.

The numerical simulation of particle trajectories was also conducted using COMSOL here, and the particles were set to mimic yeast cells with key parameters such as the diameter (3 μm), density (1114 kg/m^3) and sound speed (1606 m/s) (Hawkes et al. 1997). We studied the motion of 8100 particles suspended in water and distributed evenly at the initial time $t=0$. The quasi-stable particle trajectory is shown in Fig. 4b, where the particles exhibit rotation patterns in two obvious areas in the localized acoustic streaming field. The simulated particle trajectory around the gas-liquid interface is similar to the moving trail of a comet, which is approximately an elliptical trajectory with long-to-short axis ratio about 2. As the acoustic streaming speed near the gas-liquid interface is relatively larger, there is an acceleration process when micro particles move near the bubble radiation surface. With the increase of the bubble oscillation amplitude, micro particles far from the bubble-induced acoustic streaming region may leave from the influence range of the local vortex field under the action of centrifugal force, which is consistent with the observed rotation phenomenon of yeast cell cluster in the following experiment.

Experiments were conducted with yeast cells to visualize the streamline of bubble-induced acoustic streaming vortices. After yeast cell suspension was injected into the microfluidic chamber, the piezoelectric buzzer started vibrating, and we observed two counter-rotating bubble-induced acoustic streaming vortices around the gas-liquid interface immediately drove yeast cells to move with the fluid flow. The bubble with a small amount yeast cells which display the flow direction of acoustic streaming vortices is shown in Fig. 4c. The bubble with a large amount of cells depicting the vortex distribution is shown in Fig. 4d (see also Video 1 in supplementary material). The experimental results of the yeast trajectory are in good agreement with the simulation results. Furthermore, the vortex pattern produced by each trapped bubble is clearly visualized, and the existence of adjacent horseshoe structures has little influence on the bubble-induced acoustic streaming vortices. In comparison with Figs. 4b and d, it was found that the maximum size of yeast cell cluster observed in the experiment is about 70 μm , which is similar to the calculated long axis of elliptical trajectory of micro particles.

The vortex rotation speed and axis can be changed by modulating the applied voltage or frequency, which

corresponds to the gas-liquid interface vibration amplitude and mode. According to our experimental results and other groups' papers (Ahmed et al. 2016; Paul et al. 2007; Rallabandi et al. 2014), the vortex rotation speed is proportional to the second power of the input voltage at a certain frequency. As the input frequency increases, the gas-liquid interfaces shift from lower-order simple vibration modes to higher-order complex vibration modes, resulting that the vortex center or axis is not unalterable. As the applied voltage increases, particles far away from the vortex center may escape from the vortex, move with the convection flow field among multiple bubbles, and finally be captured by another bubble-induced acoustic streaming vortex. Thus, in order to ensure cells to stably rotate in the vortex center and facilitate 3D reconstruction of cellular morphology in the following work, the input voltage of piezoelectric buzzer should not be set too high. In our experiment, it was set to be 1–10 V_{pp} .

3.3 Simultaneous rotation of massive HeLa cells and cell clumps

Different concentrations of HeLa cell suspensions in PBS solution were introduced into the microfluidic chamber at a propulsion speed of 0.2 mm/s (or flow rate of 40 nL/s). Due to the existence of dam-like horseshoe structure array, overcrowded cells would partially clog at the entrance of the microfluidic chamber. On the other hand, however, low concentration of cells would not spread out cells around all the arrays or guarantee effective cell trapping by bubble-induced acoustic streaming vortices, such that a large number of horseshoe structures were wasted without any cell rotation. After many trials, we finally adopted a cell concentration of 500,000 cells/ mL and realised that one or two cells or cell clumps rotated in the vicinity of the gas-liquid interfaces for 70% horseshoe structures. Once the piezoelectric buzzer was turned on, the HeLa cell or cell clump within the range of bubble-induced acoustic streaming field was gradually attracted towards the vortex center under the combined action of the radiation force and acoustic streaming induced drag force of an oscillating micro-bubble. Using low-magnification objective (4x) for the microscope, we observed simultaneous rotation of cells dispersed around the horseshoe array (Fig. 5a, see also supplementary Video 2), demonstrating the high-throughput advantage of the device.

In-plane and out-of-plane rotational manipulation of single HeLa cells and cell clumps were demonstrated as image sequences in Figs. 5b-d, respectively (see also supplementary Videos 3–5). The angular speed of cell rotation caused by the acoustic streaming vortex depends on the oscillation intensity of the travelling surface acoustic field, which is controlled by changing the voltage applied to the piezoelectric buzzer. Rotational rates of HeLa cells or cell clumps reached 120 rpm (2 rev/s) in microfluidic chamber when the applied

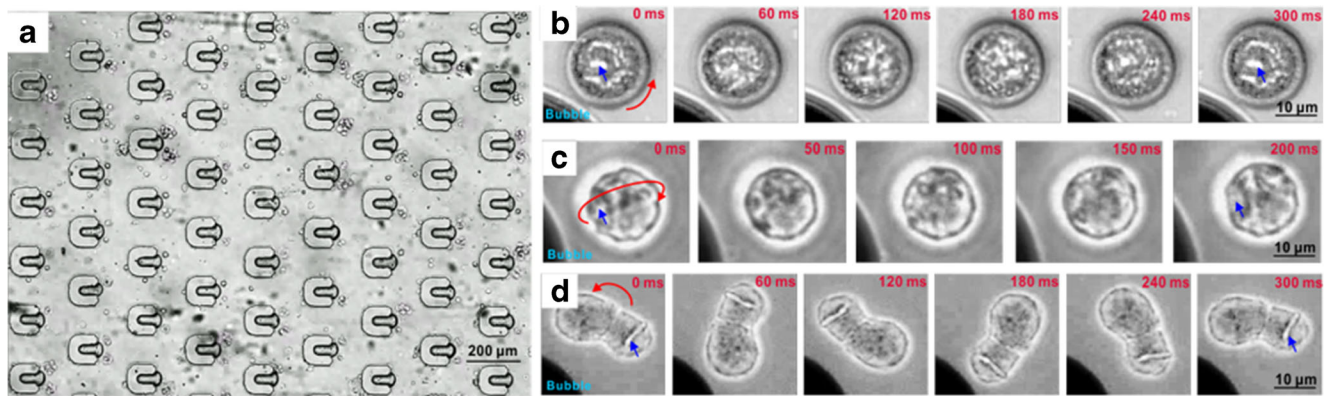


Fig. 5 Rotational manipulation of single HeLa cells or cell clumps. Note the blue arrows represent the feature points of HeLa cells to indicate one revolution. **(a)** Simultaneous rotation of massive cells. **(b)** In-plane

rotation of single cell. **(c)** Out-of-plane rotation of single cell. **(d)** In-plane rotation of a cell clump

voltage was 5 V. The rotation axes of cells or cell clumps are dependent on the streamlines of in-plane and out-of-plane vortices near the gas-liquid interfaces, which is controlled by modulating the frequency applied to the piezoelectric buzzer. With the increase of input frequency, the gas-liquid interface of the same bubble switches from lower-order simple vibration modes (commonly corresponding to in-plane cell rotation) to higher-order complex ones (commonly corresponding to out-of-plane cell rotation). The shape heterogeneity of different gas-liquid interfaces also affects available frequency points for in-plane or out-of-plane cell rotation as described below. As expected, the rotation axes of manipulated bio-samples in the center of vortices are independent on the object shape and size, which is beneficial to stably control the rotational manipulation of diverse bio-samples.

According to the existing literatures (Ahmed et al. 2016; Läubli et al. 2017, 2019), out-of-plane cell rotation mainly depends on the shape heterogeneity of gas-liquid interface along the z direction, while in-plane cell rotation depends on the gas-liquid interface curvature along the y direction. For the quasi-planar microfluidic chamber, the length ratio between z and y axes of a trapped micro-bubble is about 1:2.5. Thus, the frequency points available for out-of-plane cell rotation induced by gas-liquid interface oscillation along the z direction are fewer than those for in-plane cell rotation during the frequency modulation. Interestingly, we found that when the PDMS cover was not strongly bonded to the glass substrate, residual gas would permeate into the gaps between the PDMS cover and substrate, resulting in obvious heterogeneity of micro-bubbles along the z direction. In this case, it was easier to realise the out-of-plane cell rotation in the microfluidic chamber by modulating the frequency of piezoelectric excitation. According to our experimental observation, the out-of-plane cell rotation axis is not always in the xy plane, indicating that the in-plane and out-of-plane vortices couple with each other in some cases.

Currently due to the limitation of our microscope, we are not able to achieve both wide field of view and high

magnification in imaging the rotating cells. To really take the high-throughput advantage of this device, one may use advanced imaging technology (Fan et al. 2019) that can offer both wide view ($\sim 2 \times 2 \text{ cm}^2$) and high resolution ($\sim 1 \text{ } \mu\text{m}/\text{pixel}$) in real time. Optimization of the array structure and microfluidic channels may also be helpful to ensure the high-throughput by enhancing the bubble formation and cell dispersion uniformity in the array.

3.4 3D reconstruction of cellular morphology and geometric measurement

Out-of-plane rotation provides the inverted microscopy with a feasible and reproducible method of 3D reconstruction of cellular morphology. Based on the supplementary Video 4 of out-of-plane cell rotation, a series of cell contours can be extracted and used for 3D morphology reconstruction. During the course of image acquisition, 40x objective lens was used to enable high image resolution of the contours. By decreasing the input voltage of piezoelectric buzzer, the cell rotation speed was maintained as low as possible in order to minimize the cell rotation angular displacement between each two contour images. The maximum frame rate (90 Hz) of the camera was also used during the video recording process. Enabled by the obtained 3D morphology, the geometric parameters of HeLa cells, such as surface area, volume, ellipticity, and roughness were calculated.

Standard alpha-shape algorithm (Zheng et al. 2015) was used to reconstruct the 3D cellular morphology. To assess the accuracy of reconstruction, we also followed the reported model projection approach and found the relative error was 1/36 in theory. This indicates a good fidelity of the reconstructed morphology. A morphology reconstruction example of a HeLa cell with 347 image frames recorded at an angular displacement of 1.04° is shown in Fig. 6a. The video recording the cell rotation process was converted into a sequence of individual image frames. Every grayscale image was thresholded into a binary

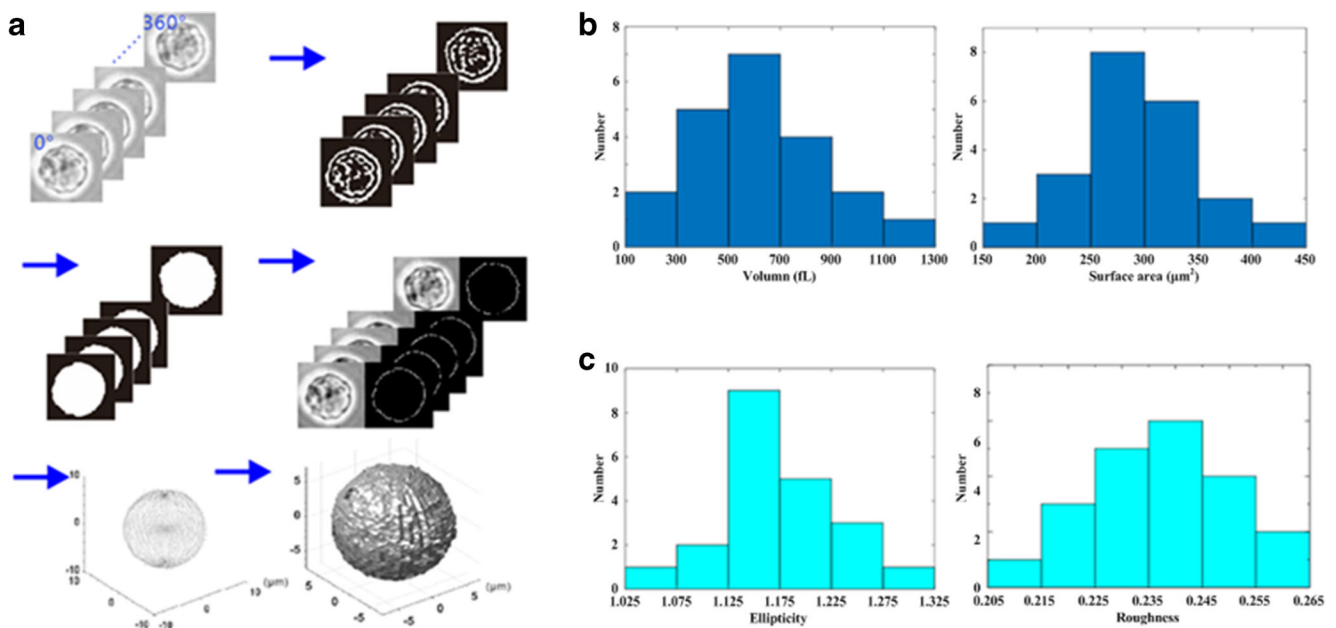


Fig. 6 3D reconstruction of cellular morphology and geometric measurement results of HeLa cells. (a) The processing procedure for 3D reconstruction of cellular morphology. (b) Volume and surface area. (c) Ellipticity and roughness

image, and the threshold value was determined such that the cell contours could be adequately distinguished from the background. Cell contours were extracted from the series of binary images, and every point on the contour had its own 3D coordinate. In practice, we extracted the contour point coordinates from several rounds of out-of-plane rotation to eliminate the background noise. All of the extracted contour points were used to sketch a point cloud, from which the 3D extracellular morphology could be reconstructed containing optimized triangles for surface smoothing. A video consisting of the reconstruction process and the reconstructed cell model is shown in the supplementary material (see supplementary Video 6). More detailed information of the extracellular morphology can be revealed by increasing the camera frame rate and lowering the cell rotation speed.

The reconstructed 3D extracellular morphology could be applied to calculate the geometric parameters of the HeLa cell. Based on our horseshoe structure array design, it is convenient to select multiple HeLa cells for 3D reconstruction on one microfluidic chip. The surface area and volume of 21 HeLa cells were calculated, and the histogram is plotted in Fig. 6b. The averaged surface area and volume of HeLa cells is $275.28 \mu\text{m}^2$ and 578.01 fL , respectively. Further research on the cell ellipticity and roughness was carried on by fitting the 3D point cloud of cell morphology as a tri-axial ellipsoid model. Ellipticity is defined as the length ratio of the longest axis to the shortest axis, while roughness is defined as the root mean squared error of the fitting. The ellipticity and roughness of 21 HeLa cells were calculated, and the histogram is shown in Fig. 6c. The averaged ellipticity and roughness of HeLa

cells is 1.14 and 0.238, respectively. These values are highly consistent with our previous measurement results obtained when the cell was under electro-rotation (Huang et al. 2018a).

4 Conclusion

A bubble-array-based method is proposed to capture and rotate massive cells or cell clumps simultaneously to improve the efficiency of acoustofluidic cell rotation and analysis. Bubble homogeneity and cell trapping are dramatically improved by modifying the horseshoe structure and microfluidic settings. Under the ultrasonic excitation, acoustic streaming vortices generated near the gas-liquid interfaces of the trapped bubbles can trap and rotate bio-samples, including yeast and HeLa cells. Cell rotation speed and axis were demonstrated by modulating the oscillation amplitude and frequency of micro-bubbles, respectively. Through a stack of 2D contour image frames obtained from out-of-plane HeLa cell rotation, the 3D morphology was reconstructed to collect cellular geometric parameters like surface area, volume, ellipticity, and roughness. Compared with mechanical, hydrodynamic, electromagnetic, and optical methods, the low-cost acoustofluidic platform here is applicable in the field of single cell manipulation and analysis, with such advantages as little physiological damage, contactless manipulation, low dependence on biophysical properties of samples.

Acknowledgements This work was supported by the NSFC (no. 61774095, 21727813, 11904117), and the National Key R&D Program (no. 2016YFC0900200).

Compliance with ethical standards

Conflict of interest The authors declare no competing financial interests.

References

- D. Ahmed, X. Mao, J. Shi, B.K. Juluri, T.J. Huang, A millisecond micromixer via single-bubble-based acoustic streaming. *Lab Chip* **9**, 2738–2741 (2009)
- D. Ahmed, C.Y. Chan, S.C.S. Lin, H.S. Muddana, N. Nama, S.J. Benkovic, T.J. Huang, Tunable, pulsatile chemical gradient generation via acoustically driven oscillating bubbles. *Lab Chip* **13**, 328–331 (2013)
- D. Ahmed, H.S. Muddana, M. Lu, J.B. French, A. Ozcelik, Y. Fang, P.J. Butler, S.J. Benkovic, A. Manz, T.J. Huang, Acoustofluidic chemical waveform generator and switch. *Anal. Chem.* **86**, 11803–11810 (2014)
- D. Ahmed, M. Lu, A. Nourhani, P.E. Lammert, Z. Stratton, H.S. Muddana, V.H. Crespi, T.J. Huang, Selectively manipulable acoustic-powered microswimmers. *Sci. Rep.* **5**, 9744 (2015)
- D. Ahmed, A. Ozcelik, N. Bojanala, N. Nama, A. Upadhyay, Y. Chen, W. Hanna-Rose, T.J. Huang, Rotational manipulation of single cells and organisms using acoustic waves. *Nat. Commun.* **7**, 11085 (2016)
- L. Alberdi, S. Méresse, Single-cell analysis: Understanding infected cell heterogeneity. *Virulence* **8**, 605–606 (2017)
- P. Benhal, J.G. Chase, P. Gaynor, B. Oback, W. Wang, AC electric field induced dipole-based on-chip 3D cell rotation. *Lab Chip* **14**, 2717–2727 (2014)
- P. Benhal, G. Chase, P. Gaynor, B. Oback, W. Wang, Multiple-ylindrical electrode system for rotational electric field generation in particle rotation applications. *Int. J. Adv. Robot. Syst.* **12**(7), 84 (2015)
- N. Bertin, T.A. Spelman, O. Stephan, L. Gredy, M. Bouriau, E. Lauga, P. Marmottant, Propulsion of bubble-based acoustic microswimmers. *Phys Rev. Appl.* **4**, 064012 (2015)
- H. Bruus, Acoustofluidics 2: Perturbation theory and ultrasound resonance modes. *Lab Chip* **12**, 20–28 (2012)
- F. Buettner, K.N. Natarajan, F.P. Casale, V. Proserpio, A. Scialdone, F.J. Theis, S.A. Teichmann, J.C. Marioni, O. Stegle, Computational analysis of cell-to-cell heterogeneity in single-cell RNA-sequencing data reveals hidden subpopulations of cells. *Nat. Biotechnol.* **33**, 155–160 (2015)
- H. Chen, Y. Gao, K. Petkovic, S. Yan, M. Best, Y. Du, Y. Zhu, Reproducible bubble-induced acoustic microstreaming for bead disaggregation and immunoassay in microfluidics. *Microfluid. Nanofluid.* **21**, 30 (2017)
- Y. Cheng, Y. Wang, Z. Ma, W. Wang, X. Ye, A bubble- and clogging-free microfluidic particle separation platform with multifiltration. *Lab Chip* **16**(23), 4517–4526 (2016)
- Y. Cheng, Y. Wang, Z. Wang, H. Liang, M. Bi, W. Xu, W. Wang, X. Ye, A mechanical cell disruption microfluidic platform based on an on-chip micropump. *Biomicrofluidics* **11**(2), 024112 (2017)
- C. Chindam, N. Nama, M.I. Lapsley, F. Costanzo, T.J. Huang, Theory and experiment on resonant frequencies of liquid-air interfaces trapped in microfluidic devices. *J. Appl. Phys.* **114**, 194503 (2013)
- W. Cui, W. Pang, Y. Yang, T. Li, X. Duan, Theoretical and experimental characterizations of gigahertz acoustic streaming in microscale fluids. *Nanotechnology and Precision Engineering* **2**(1), 15–22 (2019)
- E.M. Darling, S. Zauscher, J.A. Block, F. Guilak, A thin-layer model for viscoelastic, stress-relaxation testing of cells using atomic force microscopy: Do cell properties reflect metastatic potential? *Biophys. J.* **92**, 1784–1791 (2007)
- D. Di Carlo, K.H. Jeong, L.P. Lee, Reagentless mechanical cell lysis by nanoscale barbs in microchannels for sample preparation. *Lab Chip* **3**, 287–291 (2003)
- X. Ding, S.C.S. Lin, B. Kiraly, H. Yue, S. Li, I.K. Chiang, J. Shi, S.J. Benkovic, T.J. Huang, On-chip manipulation of single microparticles, cells, and organisms using surface acoustic waves. *P. Natl. Acad. Sci. U. S. A.* **109**, 11105–11109 (2012)
- J. Fan, J. Suo, J. Wu, H. Xie, Y. Shen, F. Chen, G. Wang, L. Cao, G. Jin, Q. He, T. Li, G. Luan, L. Kong, Z. Zheng, Q. Dai, Video-rate imaging of biological dynamics at centimetre scale and micrometre resolution. *Nat. Photonics*, published online, <https://doi.org/10.1038/s41566-019-0474-7> (2019)
- Y. Feng, H. Liang, P. Zhao, F. Liang, W. Wang, A microfluidic device integrating impedance flow cytometry and electric impedance spectroscopy for high-efficiency single-cell electrical property measurement. *Anal. Chem.* **91**(23), 15204–15212 (2019)
- N. Garg, T.M. Westerhof, V. Liu, R. Liu, E.L. Nelson, A.P. Lee, Whole-blood sorting, enrichment and *in situ* immunolabeling of cellular subsets using acoustic microstreaming. *Microsyst. Nanoeng.* **4**, 17085 (2018)
- A. Ghanbari, V. Nock, S. Johari, R. Blaikie, X.Q. Chen, W. Wang, A micropillar-based on-chip system for continuous force measurement of *J. Micromech. Microeng.* **22**(9), 095009 (2012)
- D.R. Gossett, H.T. Tse, J.S. Dudani, K. Goda, T.A. Woods, S.W. Graves, D. Di Carlo, Inertial manipulation and transfer of microparticles across laminar fluid streams. *Small* **8**, 2757–2764 (2012)
- B. Gupta, P. Rezai, Microfluidic approaches for manipulating, imaging, and screening *C. elegans*. *Micromachines* **7**(123) (2016)
- J.J. Hawkes, M.S. Limaye, W.T. Coakley, Filtration of bacteria and yeast by ultrasound-enhanced sedimentation. *J. Appl. Microbiol.* **82**, 39–47 (1997)
- W. He, H. Liang, Y. Feng, F. Liang, W. Ding, W. Wang, Highly integrated microfluidic device for cell pairing, fusion and culture. *Biomicrofluidics* **13**(5), 054109 (2019)
- N. Hu, J. Yang, S.W. Joo, A.N. Banerjee, S. Qian, Cell electrofusion in microfluidic devices: A review. *Sensor. Actuat. B-Chem.* **178**, 63–85 (2013)
- L. Huang, L. Tu, X. Zeng, L. Mi, X. Li, W. Wang, Study of a Microfluidic Chip Integrating Single Cell Trap and 3D Stable Rotation Manipulation. *Micromachines* **7**(8) 141 (2016)
- L. Huang, S. Bian, Y. Cheng, G. Shi, P. Liu, X. Ye, W. Wang, Microfluidics cell sample preparation for analysis: Advances in efficient cell enrichment and precise single cell capture. *Biomicrofluidics* **11**, 011501 (2017)
- L. Huang, P. Zhao, W. Wang, 3D cell electrorotation and imaging for measuring multiple cellular biophysical properties. *Lab Chip* **18**, 2359–2368 (2018a)
- L. Huang, P. Zhao, J. Wu, H.S. Chuang, W. Wang, On-demand dielectrophoretic immobilization and high-resolution imaging of *C. elegans* in microfluids. *Sensor. Actuat. B-Chem* **259**, 703–708 (2018b)
- L. Huang, W. Wang, 3D Electro-Rotation of Single Cells. *Synthesis Lectures on Biomedical Engineering* **14**(2) i–119 (2019)
- D. Jin, B. Deng, J.X. Li, W. Cai, L. Tu, J. Chen, Q. Wu, W.H. Wang, A microfluidic device enabling high-efficiency single cell trapping. *Biomicrofluidics* **9**(1), 014101 (2015)
- S. Johari, V. Nock, M.M. Alkaiji, W. Wang, On-chip analysis of *C. elegans* muscular forces and locomotion patterns in microstructured environments. *Lab Chip* **13**(9), 1699 (2013)
- B.L. Khoo, P.K. Chaudhuri, N. Ramalingam, D.S.W. Tan, C.T. Lim, M.E. Warkiani, Single-cell profiling approaches to probing tumor heterogeneity. *Int. J. Cancer* **139**, 243–255 (2016)
- H. Kimura, Y. Sakai, T. Fujii, Organ/body-on-a-chip based on microfluidic technology for drug discovery. *Drug Metab. Pharmacok.* **33**, 43–48 (2018)

- N.F. Läubli, N. Shamsudhin, D. Ahmed, B.J. Nelson, Controlled three-dimensional rotation of single cells using acoustic waves. *Procedia CIRP* **65**, 93–98 (2017)
- N.F. Läubli, N. Shamsudhin, H. Vogler, G. Munglani, U. Grossniklaus, D. Ahmed, B.J. Nelson, 3D manipulation and imaging of plant cells using acoustically activated microbubbles. *Small Methods* **3**, 1800527 (2019)
- H. Lee, Y. Liu, R.M. Westervelt, D. Ham, IC/microfluidic hybrid system for magnetic manipulation of biological cells. *IEEE J. Solid-St. Circ.* **41**, 1471–1480 (2006)
- J. Lei, Formation of inverse Chladni patterns in liquids at microscale: Roles of acoustic radiation and streaming-induced drag forces. *Microfluid. Nanofluid.* **21**, 50 (2017)
- J. Lei, M. Hill, C.P.L. Albarrán, P. Glynne-Jones, Effects of micron scale surface profiles on acoustic streaming. *Microfluid. Nanofluid.* **22**, 140 (2018)
- S.J. Lighthill, Acoustic streaming. *J. Sound Vib.* **61**, 391–418 (1978)
- R.H. Liu, J. Yang, M.Z. Pindera, M. Athavale, P. Grodzinski, Bubble-induced acoustic micromixing. *Lab Chip* **2**, 151–157 (2002)
- W. Liu, Y. Hou, H. Chen, H. Wei, W. Lin, J. Li, M. Zhang, F. He, Y. Jiang, Sample preparation method for isolation of single-cell types from mouse liver for proteomic studies. *Proteomics* **11**, 3556–3564 (2011)
- L. Mi, L. Huang, J. Li, G. Xu, Q. Wu, W. Wang, A fluidic circuit based, high-efficiency and large-scale single cell trap. *Lab Chip* **16**(23), 4507–4511 (2016)
- F. Mannello, D. Ligi, M. Magnani, Deciphering the single-cell omic: Innovative application for translational medicine. *Expert Rev. Proteomics* **9**, 635–648 (2012)
- A. Marin, M. Rossi, B. Rallabandi, C. Wang, S. Hilgenfeldt, C.J. Kähler, Three-dimensional phenomena in microbubble acoustic streaming. *Phys. Rev. Appl.* **3**, 041001 (2015)
- P. Marmottant, M. Versluis, N.D. Jong, S. Hilgenfeldt, D. Lohse, High-speed imaging of an ultrasound-driven bubble in contact with a wall: “Narcissus” effect and resolved acoustic streaming. *Exp. Fluids* **41**, 147–153 (2006)
- B.A. Merrick, R.E. London, P.R. Bushel, S.F. Grissom, R.S. Paules, Platforms for biomarker analysis using high-throughput approaches in genomics, transcriptomics, proteomics, metabolomics, and bioinformatics. *IARC Sci. Publ.* **121** (2011)
- S. Mohammadi, V. Ravindra, D.F. Gleich, A. Grama, A geometric approach to characterize the functional identity of single cells. *Nat. Commun* **9**(1516) (2018)
- M. Ozkan, M. Wang, C. Ozkan, R. Flynn, S. Esener, Optical manipulation of objects and biological cells in microfluidic devices. *Biomed. Microdevices* **5**, 61–67 (2003)
- P. Pan, W. Wang, R. Changhai, S. Yu, X. Liu, MEMS-based platforms for mechanical manipulation and characterization of cells. *J. Micromech. Microeng.* **27**(12), 123003 (2017)
- M.V. Patel, I.A. Nanayakkara, M.G. Simon, A.P. Lee, Cavity-induced microstreaming for simultaneous on-chip pumping and size-based separation of cells and particles. *Lab Chip* **14**, 3860–3872 (2014)
- T. Paul, M. Richard, O. Andrew, Cavitation microstreaming patterns in single and multiple bubble systems. *J. Fluid Mech.* **576**, 191–233 (2007)
- V.H. Perez-Gonzalez, R.C. Gallo-Villanueva, S. Camacho-Leon, J.I. Gomez-Quiñones, J.M. Rodriguez-Delgado, S.O. Martinez-Chapa, Emerging microfluidic devices for cancer cells/biomarkers manipulation and detection. *IET Nanobiotechnol.* **10**, 263–275 (2016)
- Z. Qiu, T. Long, H. Liang, T. Zhu, V. Nock, E. Yu, X. Liu, W. Wang, An integrated platform enabling optogenetic illumination of neurons and muscular force measurement in microstructured environments. *Biomicrofluidics* **9**(1), 014123 (2015)
- B. Rallabandi, C. Wang, S. Hilgenfeldt, Two-dimensional streaming flows driven by sessile semicylindrical microbubbles. *J. Fluid Mech.* **739**, 57–71 (2014)
- M.S. Rocha, O.N. Mesquita, New tools to study biophysical properties of single molecules and single cells. *An. Acad. Bras. Ciênc.* **79**, 17–28 (2007)
- Q. Tang, P. Liu, J. Hu, Analyses of acoustofluidic field in ultrasonic needle-liquid-substrate system for micro-/nanoscale material concentration. *Microfluidics and Nanofluidics* **22**(46) (2018)
- M. Tellez-Gabriel, B. Ory, F. Lamoureux, M.F. Heymann, D. Heymann, Tumour heterogeneity: The key advantages of single-cell analysis. *Int. J. Mol. Sci.* **17**, E2142 (2016)
- R. Thameem, B. Rallabandi, S. Hilgenfeldt, Particle migration and sorting in microbubble streaming flows. *Biomicrofluidics* **10**, 014124 (2016)
- S. Torino, M. Iodice, I. Rendina, G. Coppola, E. Schonbrun, A microfluidic approach for inducing cell rotation by means of hydrodynamic forces. *Sensors* **16**, 1326 (2016)
- L. Tu, X. Li, S. Bian, Y. Yu, J. Li, L. Huang, P. Liu, Q. Wu, W. Wang, Label-free and real-time monitoring of single cell attachment on template-stripped plasmonic nano-holes. *Scientific Reports* **7**(1) (2017)
- L. Tu, L. Huang, W. Wang, A novel micromachined Fabry-Perot interferometer integrating nano-holes and dielectrophoresis for enhanced biochemical sensing. *Biosensors and Bioelectronics* **127**, 19–24 (2019)
- A. Urbansky, P. Ohlsson, A. Lenshof, F. Garofalo, S. Scheduling, T. Laurell, Rapid and effective enrichment of mononuclear cells from blood using acoustophoresis. *Sci. Rep.* **7**, 17161 (2017)
- M.M. Villone, P. Memmolo, F. Merola, M. Mugnano, L. Miccio, P.L. Maffettone, P. Ferraro, Full-angle tomographic phase microscopy of flowing quasi-spherical cells. *Lab Chip* **18**, 126–131 (2018)
- D. Wang, S. Bodovitz, Single cell analysis: the new frontier in ‘omics’. *Trends Biotechnol* **28**, 281–290 (2010)
- C. Wang, S.V. Jalikop, S. Hilgenfeldt, Size-sensitive sorting of microparticles through control of flow geometry. *Appl. Phys. Lett.* **99**, 034101 (2011)
- C. Wang, S.V. Jalikop, S. Hilgenfeldt, Efficient manipulation of microparticles in bubble streaming flows. *Biomicrofluidics* **6**, 12801 (2012)
- C. Wang, B. Rallabandi, S. Hilgenfeldt, Frequency dependence and frequency control of microbubble streaming flows. *Phys. Fluids* **25**, 022002 (2013)
- K. Wang, X.H. Sun, Y. Zhang, T. Zhang, Y. Zheng, Y.C. Wei, P. Zhao, D.Y. Chen, H.A. Wu, W.H. Wang, R. Long, J.B. Wang, J. Chen, Characterization of cytoplasmic viscosity of hundreds of single tumour cells based on micropipette aspiration. *R. Soc. Open Sci.* **6**(3), 181707 (2019)
- Y. Xie, D. Ahmed, M.I. Lapsley, S.C.S. Lin, A.A. Nawaz, L. Wang, T.J. Huang, Single-shot characterization of enzymatic reaction constants K_m and k_{cat} by an acoustic-driven, bubble-based fast micromixer. *Anal. Chem.* **84**, 7495–7501 (2012)
- Y. Xie, D. Ahmed, M.I. Lapsley, M. Lu, S. Li, T.J. Huang, Acoustofluidic relay: Sequential trapping and transporting of microparticles via

- acoustically excited oscillating bubbles. *J. Lab. Autom.* **19**, 137–143 (2014)
- Y. Xie, N. Nama, P. Li, Z. Mao, P.H. Huang, C. Zhao, F. Costanzo, T.J. Huang, Probing cell deformability via acoustically actuated bubbles. *Small* **12**, 902–910 (2016)
- S. Yazdi, A.M. Ardekani, Bacterial aggregation and biofilm formation in a vortical flow. *Biomicrofluidics* **6**, 044114 (2012)
- Z.T. Yu, K.M. Aw Yong, J. Fu, Microfluidic blood cell sorting: Now and beyond. *Small* **10**, 1687–1703 (2014)
- S. Zhang, Z. Ma, Y. Zhang, Y. Wang, Y. Cheng, W. Wang, X. Ye, On-chip immuno-agglutination assay based on a dynamic magnetic bead clump and a sheath-less flow cytometry. *Biomicrofluidics* **13**(4), 044102 (2019)
- S. Zheng, X. Wang, D. Ma, A convenient 3D reconstruction method of small objects. *Geomatics and Information Science of Wuhan University* **40**, 147–152 (2015)
- R. Zhou, C. Wang, Acoustic bubble enhanced pinched flow fractionation for microparticle separation. *J. Micromech. Microeng.* **25**, 084005 (2015)
- Q. Zhu, M. Heon, Z. Zhao, M. He, Microfluidic engineering of exosomes: Editing cellular messages for precision therapeutics. *Lab Chip* **18**, 1690–1703 (2018)

Publisher's note Springer Nature remains neutral with regard to jurisdictional claims in published maps and institutional affiliations.